

Two-stage melting in systems of strongly interacting Rydberg atoms

Hendrik Weimer and Hans Peter Büchler

*Institute of Theoretical Physics III, Universität Stuttgart, 70550 Stuttgart, Germany**

(Dated: February 5, 2022)

We analyze the ground state properties of a one-dimensional cold atomic system in a lattice, where Rydberg excitations are created by an external laser drive. In the classical limit, the ground state is characterized by a complete devil's staircase for the commensurate solid structures of Rydberg excitations. Using perturbation theory and a mapping onto an effective low energy Hamiltonian, we find a transition of these commensurate solids into a floating solid with algebraic correlations. For stronger quantum fluctuations the floating solid eventually melts within a second quantum phase transition and the ground state becomes paramagnetic.

PACS numbers: 05.30.Rt, 32.80.Ee, 37.10.Jk, 64.70.Rh

The quantum melting of solids is a paradigm for the manifestation of quantum fluctuations at zero temperature. This quantum phase transition is driven by the competition between the interaction energy giving rise to a crystalline structure with localized particles and the kinetic energy preferring a delocalization of the particles. The qualitative behavior of the transition can be described by the Lindemann criterion, which states that the solid melts if the fluctuations around the mean position reach a certain fraction of the lattice spacing [1]. The zero temperature melting of solids with purely repulsive interactions has been studied in detail for Wigner crystals [2], and has recently attracted large attention for dipolar system realized with polar molecules [3] and Rydberg gases [4–6]. In this Letter we study the quantum melting of crystalline phases in driven Rydberg systems.

Rapid experimental progress motivated by coherent applications like quantum computing [7] and quantum simulation [8] has pushed the field of Rydberg atoms from single-particle physics into an area where strong many-body effects are important [9–14]. Within these driven strongly interacting systems, crystalline many-body ground states have recently been proposed [4–6], where an ordered arrangement of Rydberg excitations spontaneously appears in a translationally invariant configuration of frozen atoms. The absence of a kinetic term in the microscopic Hamiltonian describing these systems requires a deeper analysis to fully understand the nature of the quantum melting of these crystalline structures. Here, Rydberg atoms in one-dimensional (1D) lattices [15] are particularly suitable to investigate the properties of Rydberg crystallization.

In this Letter, we develop an effective theory allowing to study the quantum melting of crystalline phases of strongly interacting and driven Rydberg atoms in 1D lattices and determine the complete phase diagram. In contrast to the conventional melting of crystalline solids with the quantum fluctuations driven by the kinetic energy, here, the quantum fluctuations derive from the competition between interaction energy and the external laser drive, coupling the atomic ground state to the excited

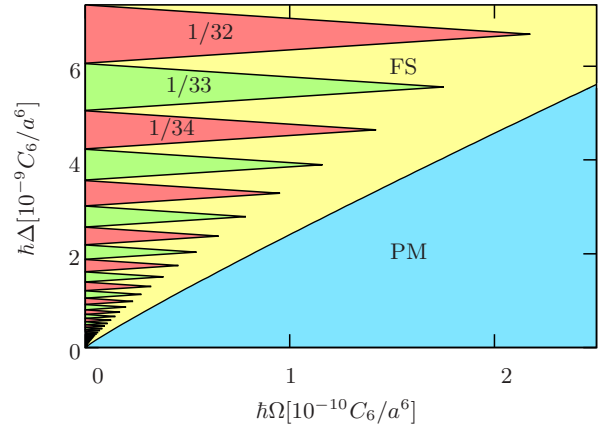


FIG. 1: Ground state phase diagram: We find commensurate solids with filling $f = p/q$ describing a complete devil's staircase for $\Omega = 0$. The lobes with $p > 1$ are not visible within this scale. For increasing Rabi frequency Ω , a quantum phase transition takes place into a gapless floating solid (FS) with algebraic correlations for the solid structure and in general incommensurate density, and eventually a second melting transition occurs into a gapped paramagnet (PM). This second transition line satisfies $\Delta \sim \Omega^{12/13}$.

Rydberg state. Deriving an effective low energy description, we find a two-stage melting: first from a commensurate solid with true long-range order to a floating solid with quasi long-range order, and finally to a paramagnetic phase, see Fig. 1. The latter transition from the floating solid to the paramagnet is in agreement with predictions from a universal scaling function [16].

We start with the microscopic Hamiltonian describing the driven Rydberg system: Rydberg excitations are created by two-photon processes via an intermediate atomic level that can be adiabatically eliminated. Consequently, the internal structure of the atoms can be treated as a single hyperfine ground state $|g\rangle$ and a single Rydberg level $|e\rangle$, giving rise to a spin 1/2 description. The coupling between the two states by an external laser field is given by the Rabi frequency Ω and the detuning Δ . The interactions between the Rydberg states are described

by a repulsive van der Waals interaction with a C_6 coefficient. Here, we focus on a 1D setup, where the atoms are trapped in a lattice with lattice spacing a . Using the Pauli matrices $\sigma_\alpha^{(i)}$, the Hamiltonian in the rotating frame after applying the rotating wave approximation reads

$$H = -\frac{\hbar\Delta}{2} \sum_i \sigma_z^{(i)} + \frac{\hbar\Omega}{2} \sum_i \sigma_x^{(i)} + \frac{C_6}{a^6} \sum_{j<i} \frac{P_{ee}^{(i)} P_{ee}^{(j)}}{(i-j)^6} \quad (1)$$

with $P_{ee}^{(i)} = (1 + \sigma_z^{(i)})/2$ [17]. Incoherent processes such as spontaneous emission are much slower than typical experimental timescales [7] and can be ignored. In addition, it is important to note that 1D lattices suitable for Rydberg excitations can be realized using deep optical lattices [18], optical [10, 11] and magnetic [19] microtraps, or micro-fabricated arrays of thermal vapor cells [20]. We do not require to have one single atom per lattice site; instead it is possible to work with collective degrees of freedom where a single Rydberg excitation is shared among all atoms of one lattice site. In the following we focus on the situation with a single atom per lattice site.

The derivation of the phase diagram from the microscopic Hamiltonian follows in three steps: (i) we start in the classical regime for $\Omega = 0$, and derive the devil's staircase structure of the commensurate crystal. (ii) We study the influence of the driven dynamics with $\Omega \neq 0$ within perturbation theory and derive the effective low energy Hamiltonian. (iii) For increasing number of defects, we study the effective Hamiltonian within mean-field theory and establish the transition into the paramagnetic phase.

For $\Omega = 0$ there are no quantum fluctuations, i.e., the Hamiltonian is purely classical. The ground state for $\Delta > 0$ follows a complete devil's staircase of crystalline configurations with different commensurate lattice spacings [21, 22]. The stability of each crystalline phase with a rational filling factor $f = p/q$ is determined by the vanishing of the single particle energy gap, i.e., when it is energetically favorable to insert or remove one Rydberg excitation. For each f we can calculate the detuning Δ_0 in the center of the lobe and its width Δ_w , which leads in the strongly interacting regime with $f \ll 1$ to

$$\Delta_0 = \frac{7\zeta(6)C_6}{a^6} \left(\frac{p}{q}\right)^6, \quad \Delta_w = \frac{42\zeta(7)C_6}{q^7 a^6}. \quad (2)$$

Note, that the lobes with $p > 1$ are extremely small, and we will restrict the analysis in the following on the stability of the lobes with $p = 1$, i.e., $f = 1/q$.

In the following, x_i denotes the position of the i^{th} Rydberg excitation in the lattice. Then, the commensurate solid satisfies $x_{i+1} - x_i = q$. Within this notation, the lowest energy excitations are characterized that the distance between two neighboring Rydberg excitations is reduced (increased) by a lattice site, i.e., $x_{i+1} - x_i = q \mp 1$; the two types of excitations are denoted as particle (hole) excitations, respectively. Note, that these elementary excitations describe fractional spin excitations [21], as the

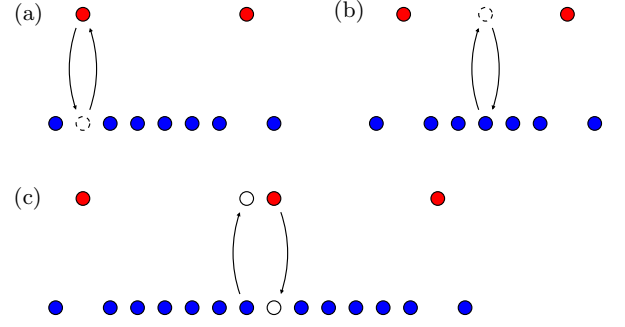


FIG. 2: Processes in second order perturbation theory. (a) Virtual annihilation of a Rydberg excitation. (b) Virtual creation of a Rydberg excitation. (c) Hopping of a crystal defect.

addition (removing) of a Rydberg excitation gives rise to $q = 1/f$ elementary excitations. Their excitation energies in the classical regime are $E_{p,h} = f\hbar(\Delta_w/2 \mp \delta\Delta)$ for particles and holes, respectively. Here, $\delta\Delta = \Delta - \Delta_0$ is the deviation of the detuning from the center of the lobe. In addition, two excitations of equal type have a repulsive interaction, while two excitations of different type are attractive.

Next, we focus on the regime with a finite drive $\Omega \neq 0$, where the system acquires a highly non-trivial dynamics. Within this regime, the melting of the commensurate crystals appears via the nucleation and subsequent condensation of defects. For a large detuning $\Delta \gg \Omega$, the system has a well-defined energy gap and we can derive an effective low-energy Hamiltonian for the defects within perturbation theory in Ω/Δ . We first restrict our treatment to three classes of states: (i) the crystalline ground state $|c\rangle$, (ii) the states $|p_i\rangle$ with a particle-like defect between the Rydberg excitation x_i and x_{i+1} , i.e., $x_{i+1} - x_i = q - 1$, and (iii) the analogous states $|h_i\rangle$ for hole-like defects. In second order perturbation theory, the effective Hamiltonian contains diagonal terms, shown in Fig. 2(a), and Fig. 2(b), while the particle (hole) defects also acquire an off-diagonal term corresponding to a hopping of the defect, see Fig. 2(c). Adding a constant energy such that $E_c = 0$ the diagonal terms take the form

$$\langle \alpha | H_{\text{eff}} | \alpha \rangle = E_\alpha + \sum_{x_i} \frac{\hbar^2 \Omega^2}{E_\alpha - E_i^{(a)}} + \sum_{j \notin \{x_i\}} \frac{\hbar^2 \Omega^2}{E_\alpha - E_j^{(b)}}.$$

Here, $E_j^{(a)}$ and $E_j^{(b)}$ correspond to the energies of the virtual levels depicted in Fig. 2(a-b), which take the form

$$E_i^{(a)} - E_\alpha = -\frac{C_6}{a^6} \sum_{x_j \neq x_i} \frac{1}{|x_i - x_j|^6} + \hbar\Delta, \quad (3)$$

$$E_j^{(b)} - E_\alpha = \frac{C_6}{a^6} \sum_{x_i} \frac{1}{|x_i - x_j|^6} - \hbar\Delta.$$

Consequently, the diagonal terms provide an additional shift in the excitation energy for the particles and holes,

which in the limit $f \ll 1$ reduces to ($\alpha = p, h$)

$$\Delta E_\alpha = \langle \alpha_i | H_{\text{eff}} | \alpha_i \rangle - \langle c | H_{\text{eff}} | c \rangle - E_\alpha = I_\alpha \frac{\hbar \Omega^2}{\Delta}, \quad (4)$$

with the dimensionless quantities $I_p \approx -I_h \approx 0.090$. The off-diagonal defect hopping for holes reduces to

$$J_h = \langle h_i | H_{\text{eff}} | h_{i\pm 1} \rangle = \frac{\hbar^2 \Omega^2}{E_h - E_i^{(c_1)}} + \frac{\hbar^2 \Omega^2}{E_h - E_i^{(c_2)}}, \quad (5)$$

where the first process annihilates a Rydberg excitation at position x_i with the subsequent creation of the Rydberg excitation at position $x_i \pm 1$, while the second term reverses the order of creation and annihilation. Finally, the corresponding term J_p for the hopping of particle defects is obtained similarly, and the evaluation of the second order processes provides $J_p = K_p \hbar \Omega^2 / \Delta$ and $J_h = K_h \hbar \Omega^2 / \Delta$ with $K_p \approx K_h \approx -7/5$. We can now derive the shape of the lobes for the commensurate solid, see Fig. 1: the nucleation of particle like defects destroying the commensurate solid takes place at the vanishing of the excitation gap, i.e., $E_p + \Delta E_p - 2J_p = 0$ and determines the upper boundary of the lobes, while the nucleation of hole like defects becomes preferable for $E_h + \Delta E_h - 2J_h = 0$, which determines the lower boundary for the lobes.

The new phase is characterized by a finite density of defects. These defects obey a strong on-site repulsion, and consequently, close to the phase transition line the density of defects is very low. This allows us to describe the qualitative behavior of the quantum phase transition within an effective spin-1 theory for the defects

$$H_{\text{eff}} = -J \sum_i [S_i^+ S_{i+1}^- + \text{h.c.}] + U (S_i^z)^2 - \mu S_i^z \quad (6)$$

with the three states $|m\rangle_i$ describing the presence of a particle ($m = 1$) or hole ($m = -1$) defect at site i . The XY interaction with $J = J_p \approx J_h$ includes the hopping of the defects and the possibility to create particle-hole pairs, while the uniaxial anisotropy $U = f \hbar \Delta_w / 2$ accounts for the cost in energy to create defects, and the chemical potential $\mu = \hbar \delta \Delta$ describes the variation in detuning. Note, that this model neglects additional weak particle-hole symmetry breaking terms, longer range interactions, higher orders in Ω / Δ perturbation theory, and the possibility to nucleate several defects at the same site. However, these additional terms will only change the quantitative behavior of the commensurate lobes.

The effective one-dimensional spin-1 model gives naturally rise to a transition from the commensurate solid with an excitation gap to a phase with algebraic correlations $\langle S_i^z S_j^z \rangle - \langle S_i^z \rangle^2 \sim 1/|i - j|^{2K}$ and linear excitation spectrum. Varying the detuning $\delta \Delta$ results in a commensurate-incommensurate transition with defects behaving as free fermions, i.e., $K = 1$, while the transition at the tip of the lobe is described by the Kosterlitz-

Thouless universality class with $K = 2$ [23]. However, the physical quantity describing the properties of the Rydberg atoms is given by the spin-spin correlation $\langle P_{ee}^{(i)} P_{ee}^{(j)} \rangle$ rather than the defect correlations $\langle S_i^z S_j^z \rangle$. Consequently, we have to provide a mapping allowing to calculate the physical quantity from the effective model. The defect density S_i^z can be expressed in terms of the position of the Rydberg atoms as $S_i^z = x_{i+1} - x_i - q$. Consequently, the total defect number $N_k = \sum_{j=0}^{i-1} S_j^z = x_k - x_0 - kq$ between the Rydberg excitation at x_0 and x_k defines the position of the k^{th} Rydberg excitation. As the system is translational invariant, we can assume without loss of generality $x_0 = 0$. Then, the correlations between the Rydberg atoms take the form

$$\langle P_{ee}^{(0)} P_{ee}^{(j)} \rangle = \frac{1}{q+n} \sum_k \langle \delta_{j, kq+N_k} \rangle = \sum_k \frac{P_k(j-kq)}{q+n} \quad (7)$$

with $n = \langle n_i \rangle$ the defect density in the effective Hamiltonian. Here, $P_k(m)$ denotes the probability distribution of N_k to find m defects. In the regime where the system is described by free fermions, the distribution function can be determined efficiently numerically at short distances using Monte-Carlo simulations with correlated random numbers [24], see Fig. 3. On the other hand, the long distance behavior can be derived within Luttinger liquid theory [25], predicting a Gaussian distribution with a mean value nk and a variance $\kappa^2 = \langle (N_k - nk)^2 \rangle = K \log(k/b)/\pi^2$; here $b \sim \pi n$ denotes a short distance cutoff. As shown in Fig. 3, this Gaussian distribution even captures the qualitative behavior on short distances. Consequently, we find that the Rydberg-Rydberg correlations oscillate with period $n+q$ and decay on short distances as $1/\sqrt{\log[j/(n+q)/b]}$, while a transition to an algebraic decay occurs at large distances, i.e.,

$$\frac{\langle P_{ee}^{(0)} P_{ee}^{(j)} \rangle - \langle P_{ee}^{(0)} \rangle^2}{\langle P_{ee}^{(0)} \rangle^2} \sim \cos \left(\frac{2\pi j}{n+q} \right) \left[\frac{(n+q)b}{j} \right]^{\frac{2K}{(n+q)^2}}$$

with $\langle P_{ee}^{(0)} \rangle = 1/(n+q)$. Therefore, we find that the transition from the commensurate solid takes place into a novel phase exhibiting quasi long-range order for the solid correlation function. As the density is in general incommensurate with the underlying lattice structure we denote this novel phase as a floating solid. It is important to note, that the crossover from the short distance regime to the algebraic decay takes place once the different terms in Eq. (7) start to overlap, i.e., $j \sim \exp[(n+q)^2/2]$. While this scale is much larger than the typical experimental scale achievable, the short distance $1/\sqrt{\log j/b}$ decay is a unique characteristic for this phase.

In the regime of large Rabi frequencies with $\Omega \gg C_6/a^6 \gg \Delta$, the spin Hamiltonian (1) reduces to the Ising model in a transverse and a longitudinal field. Then, the ground state is described by a gapped paramagnetic phase with algebraic decay of the correlations as $1/r^6$ due

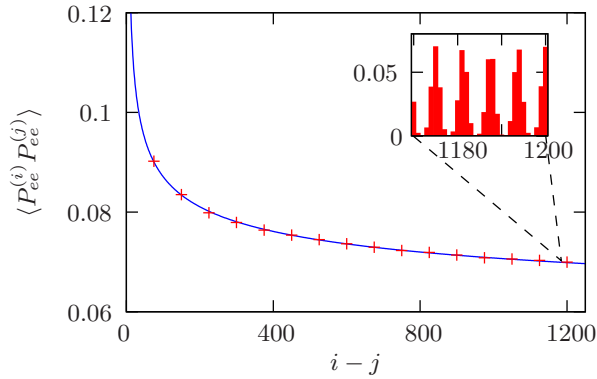


FIG. 3: Decay of the spin correlations from Monte-Carlo simulations (crosses) according to $c/\sqrt{\ln j/b'}$ (solid line) as predicted by Luttinger liquid theory ($q = 6$, $n = 0.25$). The crossover to the algebraic decay takes place at much larger distances $|i - j| \sim 10^9$. The inset shows the oscillations of the correlation function.

to the long range interaction [26]. Consequently, a second phase transition takes place from the gapless floating solid to the paramagnet.

This second transition can be seen as the breakdown of an effective theory describing the system in terms of defects, and takes place when the number of defects n_i at a site i becomes of the order of the spacing between the Rydberg atoms q . Note, that this criterion is equivalent to classical Lindemann criterion for the melting of solids [1]. The effective Hamiltonian at the commensurate density $\mu = 0$ describing the qualitative behavior for higher defect densities includes multiple defects at a site, and also allows for multiple defect hopping, i.e.,

$$H_{\text{eff}} = U \sum_i n_i^2 - J \sum_i \left[\sum_{mnp} |n\rangle\langle n+p|_i \otimes |m+p\rangle\langle m|_{i+1} \right]$$

with $|n\rangle_i$ describing the state with n defects at site i ($n < 0$ for holes and $n > 0$ for particles). Using mean field theory, we obtain for the fluctuations of the defect number $\langle n_i^2 \rangle \sim J^2/U^2$, and comparing this value with the mean spacing between the Rydberg atoms $q^2 \sim J^2/U^2$ provides the scaling $\Delta \sim \Omega^{12/13}$ for the transition line from the floating solid towards the paramagnet. Note, the influence of the underlying lattice drops out for this second transition, and the scaling agrees with the value previously derived using a universal scaling function [16]. The complete phase diagram exhibiting three different phases is sketched Fig. 1. Note that this phase diagram is also in good agreement with recent numerical results obtained for the spin Hamiltonian (1) at high fillings [6].

Experimentally, the commensurate solids are the most challenging to realize. They can be observed if the critical Rabi frequency Ω_c at the tip of the lobe is much larger than the intrinsic decoherence rates, e.g., by radiative decay. For ^{87}Rb atoms with a principle quantum number $n = 80$ and a lattice spacing $a = 266 \text{ nm}$, we

find for the $q = 32$ phase $\Omega_c = 2\pi \times 1.5 \text{ MHz}$. Note that isolated radiative decays will lead to an overall reduction in Rydberg atom density, but correlations will be largely unaffected.

Finally, the presence of a floating solid with incommensurate fillings between the commensurate solid lobes and the paramagnetic phase is highly remarkable as the underlying lattice structure is not required to stabilize this phase. Consequently, we expect that this floating solid with quasi long-range order also survives a different arrangement of the atoms; especially we expect that this phase is also present in the 'frozen' Rydberg regime [27], where the atoms are distributed randomly.

Discussions with A. Daley and J. Schachenmayer are acknowledged. The work was supported by the Deutsche Forschungsgemeinschaft (DFG) within SFB/TRR 21.

* Electronic address: hweimer@itp3.uni-stuttgart.de

- [1] H. Kleinert, *Stresses and Defects: Differential Geometry, Crystal Melting* Vol. II of *Gauge fields in condensed matter* (World Scientific, Singapore, 1989).
- [2] E. Wigner, Phys. Rev. **46**, 1002 (1934); B. Tanatar and D. M. Ceperley, Phys. Rev. B **39**, 5005 (1989).
- [3] H. P. Büchler et al., Phys. Rev. Lett. **98**, 060404 (2007); G. E. Astrakharchik et al., *ibid.* **98**, 060405 (2007).
- [4] H. Weimer et al., Phys. Rev. Lett. **101**, 250601 (2008).
- [5] T. Pohl, E. Demler, and M. D. Lukin, Phys. Rev. Lett. **104**, 043002 (2010).
- [6] J. Schachenmayer et al., New J. Phys. **12**, 103044 (2010).
- [7] M. Saffman, T. G. Walker, and K. Mølmer, Rev. Mod. Phys. **82**, 2313 (2010).
- [8] H. Weimer et al., Nature Phys. **6**, 382 (2010).
- [9] R. Heidemann et al., Phys. Rev. Lett. **99**, 163601 (2007).
- [10] E. Urban et al., Nature Phys. **5**, 110 (2009).
- [11] A. Gaëtan et al., Nature Phys. **5**, 115 (2009).
- [12] K. C. Younge et al., Phys. Rev. A **79**, 043420 (2009).
- [13] J. D. Pritchard et al., Phys. Rev. Lett. **105**, 193603 (2010).
- [14] H. Schempp et al., Phys. Rev. Lett. **104**, 173602 (2010).
- [15] B. Olmos, R. González-Férez, and I. Lesanovsky, Phys. Rev. A **79**, 043419 (2009).
- [16] R. Löw et al., Phys. Rev. A **80**, 033422 (2009).
- [17] F. Robicheaux and J. V. Hernández, Phys. Rev. A **72**, 063403 (2005).
- [18] I. Bloch, J. Dalibard, and W. Zwerger, Rev. Mod. Phys. **80**, 885 (2008).
- [19] S. Whitlock et al., New J. Phys. **11**, 023021 (2009).
- [20] H. Kübler et al., Nature Photon. **4**, 112 (2010).
- [21] P. Bak and R. Bruinsma, Phys. Rev. Lett. **49**, 249 (1982).
- [22] F. J. Burnell et al., Phys. Rev. B **80**, 174519 (2009).
- [23] W. Chen, K. Hida, and B. C. Sanctuary, Phys. Rev. B **67**, 104401 (2003).
- [24] B. F. Qaqish, Biometrika **90**, 455 (2003).
- [25] F. D. M. Haldane, Phys. Rev. Lett. **47**, 1840 (1981).
- [26] N. Schuch, J. Cirac, and M. Wolf, Comm. Math. Phys. **267**, 65 (2006).
- [27] W. R. Anderson, J. R. Veale, and T. F. Gallagher, Phys. Rev. Lett. **80**, 249 (1998).